Available Online

JOURNAL OF SCIENTIFIC RESEARCH

J. Sci. Res. **17** (2), 489-505 (2025) www.banglajol.info/index.php/JSR

Synthesis and Study the Impact of Annealing Temperature on Structural, Electrical and Gas Sensing Properties of $LaCrO_3$ Thick Films

S. B. Handge[1*], U. P. Shinde[1, 2], D. K. Halwar[1]

[1]Research Centre in Electronic Science, Mahatma Gandhi Vidyamandir's Loknete Vyankatrao Hiray Arts, Science and Commerce College, Panchavati, Nashik (422003), Affiliated to SPPU, Pune, Maharashtra, India

[2]M.J.M. Arts, Commerce and Science College, Karanjali, Tal. Peth, Dist. Nashik (422208), Affiliated to SPPU, Pune, Maharashtra, India

Received 12 September 2024, accepted in final revised form 9 March 2025

Abstract

In this work, $LaCrO_3$ nanostructure were modified with annealing temperature. The present work deals with the study of the impact of annealing temperature on the structural, electrical and gas sensing properties of $LaCrO_3$ thick films. The thick films of $LaCrO_3$ were developed on glass substrate by screen printing technique. The $LaCrO_3$ nanostructure was synthesized by sol–gel method. The characterizations were carried out by using standard tools like X-ray diffraction (XRD), energy-dispersive X-ray (EDX) and scanning electron microscopy (SEM) revealed the confirmation of a crystal structure, elemental analysis and the morphology of synthesized $LaCrO_3$ respectively. The impact of annealing temperature on selected properties of $LaCrO_3$ thick films were successfully studied. The investigation suggested that, the annealed thick films possess better results than unannealed films. The developed $LaCrO_3$ thick films were used to detect various hazardous air pollutants such as NO_2, CH_4, LPG, ethanol, NH_3 and petrol vapor. $LaCrO_3$ thick films shows maximum sensitivity to nitrous oxide gas at operating temperature 160 °C. The films also demonstrated quick response and recovery time.

Keywords: Nanostructure; Thick films; Sol–gel; Nanoparticles; Air pollutants; Sensitivity; Recovery time.

doi: https://dx.doi.org/10.3329/jsr.v17i2.76139 J. Sci. Res. **17** (2), 489-505 (2025)

1. Introduction

The study of the impact of annealing temperature on metal oxide and perovskite oxide films is considered important due to its significant effects on various properties. During annealing, a material is heated to a specific temperature and then allowed to cool slowly, which leads to considerable alterations in structural, electrical, optical, physical, and gas sensing properties [1]. In terms of structural properties, crystallinity, grain size, and phase composition of films are influenced by annealing temperature. Higher temperatures have

* *Corresponding author*: somnathhandge@gmail.com

been observed to promote crystallization and grain growth, resulting in improved structural integrity and enhanced mechanical strength. In the electrical properties, variations in conductivity are induced by changes in carrier concentration, mobility, and defect states within the material due to annealing [1,2]. Through the optimization of annealing conditions, resistivity is reduced or increased, and conductivity is changed, which is key for applications in electronics and sensors. In the case of optical properties, modifications in the optical bandgap, transparency, and light absorption characteristics of oxide films are induced by annealing [2]. Controlled annealing has been reported to enhance light absorption in photovoltaic materials and improve transparency in optical coatings. Mechanical properties, such as hardness, adhesion, and thermal stability, are also influenced by annealing, making films more durable and adaptable to various environmental conditions. For gas sensing applications, surface morphology, defect density, and interaction sites available for gas molecules are affected by annealing temperature. By optimizing annealing conditions, improvements in sensitivity, selectivity, and response time of gas sensors are achieved. The significance of studying annealing temperature lies in the optimization of these properties for specific applications [3,4]. Vast differences in material characteristics have been observed under different annealing temperatures, making it essential to determine ideal conditions that maximize performance and functionality. Through this understanding, oxide films are tailored to meet the stringent requirements of diverse technological applications, including sensors, optoelectronics, catalysis, and energy storage. Therefore, detailed investigations into the effects of annealing temperature continue to provide critical insights that contribute to advancements in material science and technology [5-7].

Lanthanum chromite ($LaCrO_3$) is a perovskite oxide with a wide range of applications due to its excellent thermal stability, electrical conductivity, and catalytic properties, making it suitable for various applications, particularly in high-temperature and catalytic environments [8]. It has been observed that $LaCrO_3$ adopts a perovskite crystal structure (ABO_3), where La (Lanthanum) is positioned at the A-site, Cr (Chromium) occupies the B-site, and O (Oxygen) forms the octahedral network. The theoretical density of $LaCrO_3$ has been reported to be approximately 6.67 g/cm^3 [9]. Good mechanical strength and hardness are exhibited by $LaCrO_3$, which are considered important for structural applications. It has been found to function as a catalyst in various chemical reactions, including oxidation and reduction processes, and its catalytic activity has been shown to be modifiable by doping with other elements [10,11]. High resistance to corrosion and chemical attack has been noted, contributing to its durability in various environments. Mixed ionic and electronic conductivity has been exhibited by $LaCrO_3$, and it has been classified as a p-type semiconductor. The band gap of $LaCrO_3$ has been found to be around 3.4 eV, which influences its semiconducting behavior. Its dielectric properties have been characterized by a high dielectric constant, making it applicable in capacitor technology and dielectric materials in electronics. Moderate thermoelectric properties have been observed in $LaCrO_3$ and it has been demonstrated that doping with other elements can enhance its performance in thermoelectric devices [12]. Due to its high thermal stability, chemical resistance, and

electrical conductivity, $LaCrO_3$ has been regarded as a versatile material suitable for various advanced technological applications, especially in high-temperature environments and energy-related devices. Ongoing research continues to focus on further exploring and enhancing these properties, thereby expanding the potential applications of $LaCrO_3$ nanoparticles [13-15].

Annealing temperature is defined as the temperature at which a material, such as nanoparticles or films, is heated and maintained for a certain period to induce alterations in its physical, electrical, magnetic, optical, and chemical properties. This process has been recognized as crucial in materials science and engineering for enhancing the performance of materials for specific applications [15,16]. Therefore, the present research has been focused on investigating the impact of annealing temperature on the structural, electrical, and gas sensing properties of $LaCrO_3$ thick films, which have been developed using the screen-printing technique. In this study, a comparative analysis of the structural, electrical, and gas sensing properties of both unannealed and annealed $LaCrO_3$ thick films has been reported.

2. Materials and Methods

2.1. *Material*

The $LaCrO_3$ nanoparticles were synthesized from the chemicals without further purification. All analytical (AR) grade required chemicals were purchased. Lanthanum nitrate [La $(NO_3)_3$], chromium nitrate $Cr(NO_3)_3$, double distilled water and citric acid were purchased from Sigma enterprises , Nashik.

2.2. *Synthesis of $LaCrO_3$ nanoparticles by sol gel*

$LaCrO_3$ nanoparticles were synthesized by straightforward and less expensive sol gel method. For this synthesis we followed the same procedure according to our prior work [17,18]. The synthesis process and steps are illustrated in Fig. 1.

2.3. *Development of thick films of synthesized $LaCrO_3$ nanoparticles*

The thick films of synthesized $LaCrO_3$ nanoparticles were developed on a glass substrate. The conventional screen-printing technique was utilized for the fabrication of $LaCrO_3$ films. This technique has been noted to be cost-effective and does not require a power supply for the preparation of thick films. The synthesized $LaCrO_3$ nanoparticles or nanopowder were converted into a thixotropic paste by maintaining a standard ratio of inorganic (70 %) and organic (30 %) chemicals. The inorganic component consisted of synthesized $LaCrO_3$ nanoparticles, while the organic chemicals included butyl carbitol acetate (BCA) and ethyl cellulose (EC) [16,19]. In Fig. 2, the steps involved in the development of thick films of synthesized $LaCrO_3$ using the screen-printing technique are illustrated.

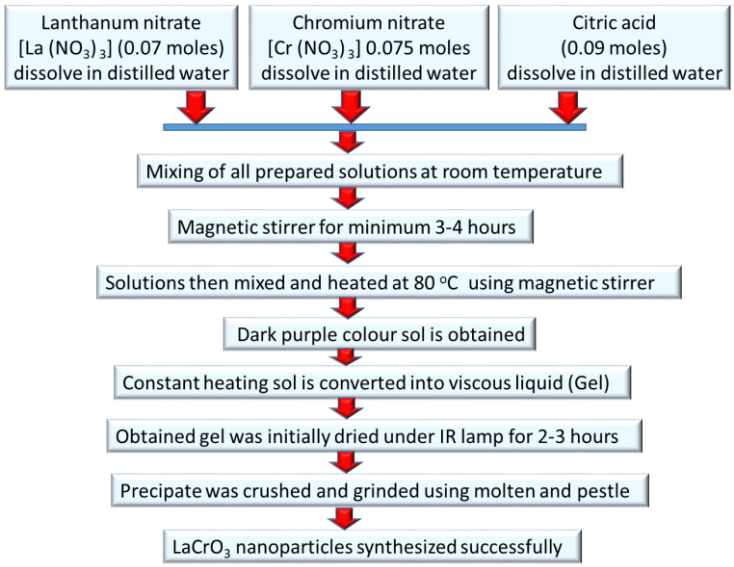

Fig. 1. Flowchart of synthesis of $LaCrO_3$ nanoparticles.

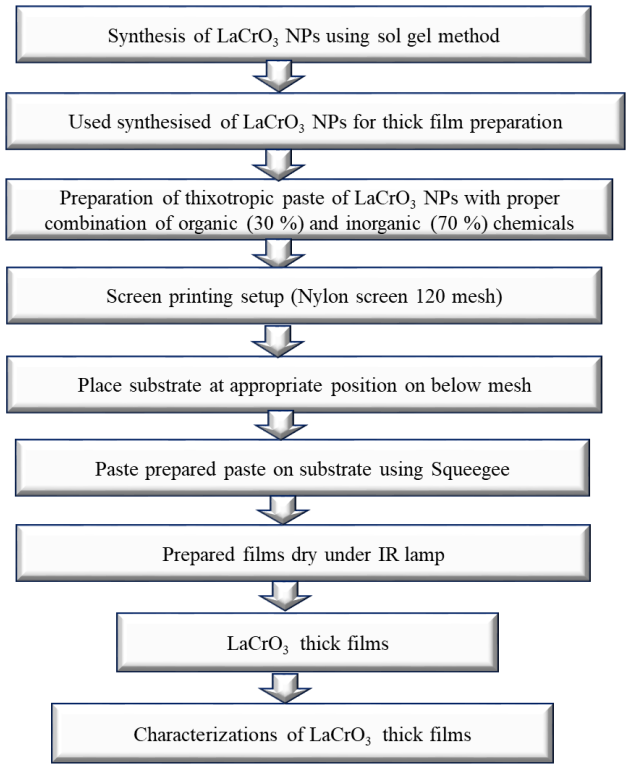

Fig. 2. Steps for development of thick films of synthesized $LaCrO_3$.

In the present research work, the prepared thick films have been categorized in two ways: first, as unannealed $LaCrO_3$ thick films, and second, as $LaCrO_3$ thick films subjected to annealing for studying its effects. The unannealed $LaCrO_3$ thick film samples have been labeled as La1, while the annealed $LaCrO_3$ thick film samples have been designated as La2. The films (La2) were annealed at a temperature of 400 °C for a duration of 3 hours using a muffle furnace.

2.4. *Characterization techniques*

The prepared unannealed and annealed thick films of $LaCrO_3$ were characterized by standard techniques or tools. The Scanning Electron Microscopy (SEM) was carried out using Model JEOL 6300(LA), Germany. The elemental analysis was carried out using energy dispersive X-ray spectrometer EDX (JEOL- JED-2300, Germany). The X-ray diffractometer was carried out using [Bruker D8, Advance, Germany] using CuKα radiation (λ=1.5409 Å). The XRD analysis was done in 2θ angle range of 20° to 80°. The thickness of films was calculated using mass difference method. The electrical parameters like resistance, resistivity, activation energy and temperature coefficient resistance (TCR) of films were measured using half bridge method. Gas sensing study was carried out using static gas sensing system.

3. Results and Discussion

3.1. *Study of structural properties of $LaCrO_3$ thick films*

3.1.1. *Scanning electron microscopy (SEM)*

The impact of annealing temperature on the morphology of $LaCrO_3$ thick films is investigated in this study by scanning electron microscopy (SEM). The SEM images of prepared $LaCrO_3$ thick films are shown in Fig. 3 at 10 K magnifications.

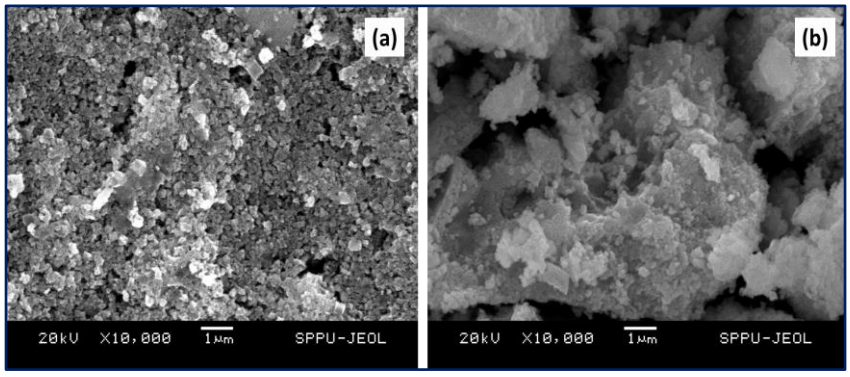

Fig. 3. SEM images of (a) unannealed and (b) annealed $LaCrO_3$ thick films.

The annealing temperature facilitate atomic diffusion, leading to grain growth and more regular grain shapes. The grains become larger, more uniform, and well-defined. This annealing process increase the porosity of film [29,30]. Annealing temperatures also promote surface smoothing as shown in Fig. 1b. Annealing temperatures lead to a more homogeneous microstructure [18,19]. Grain boundaries become fewer and less prominent as grains grow [31,32]. Fig. 1b also shows the surface of film is smoother than Fig. 1a with higher voids and porosity. The specific surface area was estimated using BET method [Eq. 1] and the diameter of spherical particles was measured using Image J software [19].

$$Sw = 6/\rho d \quad (1)$$

Where, Sw is the specific surface area, d is the diameter of the particles and ρ is the density of the particles.

The specific surface area for unannealed and annealed $LaCrO_3$ thick films was found to be 2.15 m^2/g and 5.23 m^2/g respectively. The higher surface area plays a very vital role for gas sensing mechanism, higher surface area enhanced the sensitivity and selectivity of the film sensor [32].

3.1.2. *Energy dispersive X-ray spectrometer (EDX)*

Energy Dispersive X-Ray Spectroscopy (EDS or EDX) is a chemical microanalysis technique used in conjunction with scanning electron microscopy. Fig. 4 shows the elemental composition of prepared $LaCrO_3$ thick films. The EDX spectra of unannealed and annealed $LaCrO_3$ thick films clearly indicate the presence of La, Cr, and O peaks which confirming the by adopted sol-gel method the nanoparticles of $LaCrO_3$ are successfully synthesized. The sharp peaks of oxygen and chromium was found to be at 0.4-0.8 KeV. While the characteristics peak of lanthanum was found to at in the range of 4.2-5.8 keV.

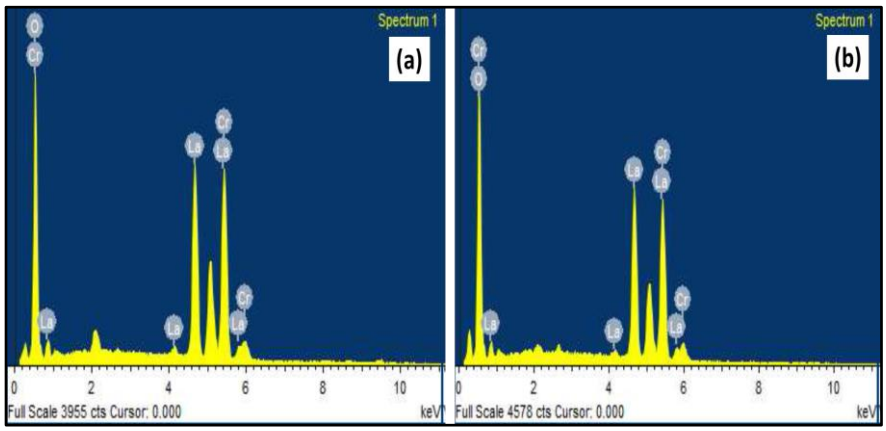

Fig. 4. EDX spectra of (a) unannealed and (b) annealed $LaCrO_3$ thick films.

The EDS spectrum of $LaCrO_3$ thick films shows its elemental composition and the weight and atomic percentage values are tabulated in Table 1.

Table 1. Elemental outcomes of unannealed and annealed $LaCrO_3$ thick films.

Sample	Elements	Weight%	Atomic%
La1	O	41.40	80.89
	Cr	15.75	09.47
	La	42.85	09.64
La2	O	37.49	78.17
	Cr	17.00	10.91
	La	45.50	10.93

By comparing the weight and atomic percentage values of unannealed and annealed $LaCrO_3$ thick films, it is observed that the weight and atomic percentage of oxygen vacancies are decreased with annealing temperature. The La2 sample shows less number of oxygen elements compare to La1 sample. It could be because of annealing temperature provide sufficient energy to the material, allowing oxygen atoms to diffuse and occupy vacant sites [20]. This process reduces the number of oxygen vacancies as the crystal structure becomes more ordered and closer to its stoichiometric composition. During annealing in an oxygen-rich environment, $LaCrO_3$ can re-oxidize, allowing oxygen atoms to fill the vacancies created during synthesis or previous treatments. This re-oxidation process is facilitated by the increased mobility of oxygen ions at higher temperatures [16,19]. This results in a decrease in both the weight and atomic percentage of oxygen vacancies as the material becomes more stoichiometric and less defective [34,35].

3.1.3. *X- ray Diffraction (XRD)*

For the analysis the structural parameters like crystallinity, structure of material, defects, stresses, homogenized, and average bulk composition of material XRD is extensively used. The XRD pattern of $LaCrO_3$ thick films is reveal in Fig. 5. It is found that, the peak intensity of La2 sample is maximum to La1 sample.

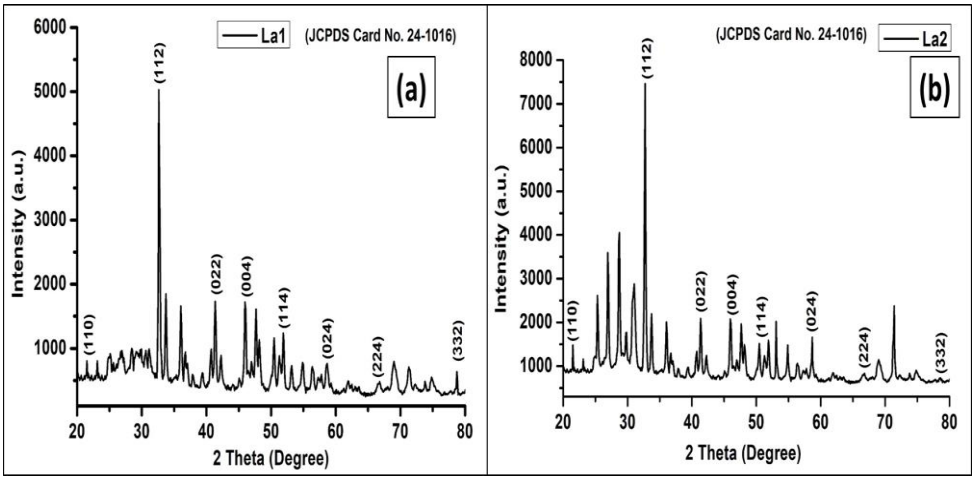

Fig. 5. XRD pattern of (a) unannealed and (b) annealed $LaCrO_3$ thick films.

The obtained results suggest that, annealing temperature improve the crystallinity of the material. The annealing temperature enhance the crystallinity of $LaCrO_3$ thick films it may be due to annealing process the energy provided allows atoms to move more freely and occupy their proper lattice positions. This leads to a more ordered crystal structure with fewer defects, resulting in sharper and more intense XRD peaks [21]. Synthesis of the desired $LaCrO_3$ was also confirmed by XRD analysis. The XRD pattern revealed in Fig. 5 illustrates broad peaks due to the nanosized of particles and matches with the reported JCPDS data card No.24-1016 [21]. It is also recorded that the position of prominent peak is shift due to annealing temperature comparing the JCPDS data [22]. The prominent peak for La1 and La2 samples was indicated by hkl plane (1 1 2) and attributing orthorhombic perovskite structures. After annealing few peak's intensity was found to be increases as shown in Fig. 5b. The obtained XRD peaks are in good agreements with the reported results. The orthorhombic structure of samples has the lattice parameters a = 5.586 Å and b = 5.488 Å, c = 7.758 Å (c/a = 1.388) respectively. The crystalline size (D) for both samples was calculated using Scherrer's equation [Eq. 2] and calculated values of crystalline size are tabulated in Table 2.

$$D = \frac{K\lambda}{\beta Cos\theta} \tag{2}$$

Where, D = Crystallite size, K = Scherrer constant (0.9), β = Full width of half maxima (FWHM), and λ = wavelength of X source.

The crystalline size of La2 sample is found to be minimum than La1 sample. Due to annealing process the crystallite size of $LaCrO_3$ thick films is deceased. The decreased size of crystallite size because of annealing temperatures can relieve internal strains in the material. While this typically leads to grain growth, in some cases, the relief of strain can lead to the breaking up of larger crystallites into smaller ones if the material structure becomes more stable in this configuration [20,21]. Restructuring to minimize surface energy, resulting in smaller crystallites. Due to reduction in size of crystallite it affects the gas sensing property because as crystallite size decreased the surface area to volume ratio increased which affect gas sensing properties of sensor. Smaller crystallites mean a larger surface area relative to volume, providing more active sites for gas adsorption [16]. More surface atoms and active sites allow for greater interaction with gas molecules, leading to higher adsorption rates. This increased surface area improves the sensor's ability to detect lower concentrations of gases, enhancing its sensitivity [20].

Table 2. Structural outcomes of unannealed and annealed $LaCrO_3$ thick films.

Sample	2 Theta	FWHM	Intensity	Crystallite size (nm)	Surface area (m^2/g)
La 1	32.53	0.2151	5029.4	40.11	2.15
La 2	32.82	0.1936	7484.3	44.59	5.23

3.2. *Study of electrical properties of $LaCrO_3$ thick films*

Converting metals into metal oxides for gas sensing applications involves several synthesis methods. These methods ensure the production of metal oxides with desired properties such as high surface area, appropriate morphology, and specific crystalline phases. The confirmation of conversion of metals into metal oxides is verify by electrical properties. The metals are positive temperature coefficient while the metal oxides are negative temperature coefficient because metal oxides are playing the role like semiconductors. The baseline resistance of a metal oxide sensor is determined by its semiconducting properties and ambient conditions [23]. To confirm the semiconducting property of synthesized and prepared $LaCrO_3$ thick films the electrical characterizations were carried out by using half bride method and static electric and gas sensing system shown in Fig. 6 [20,24].

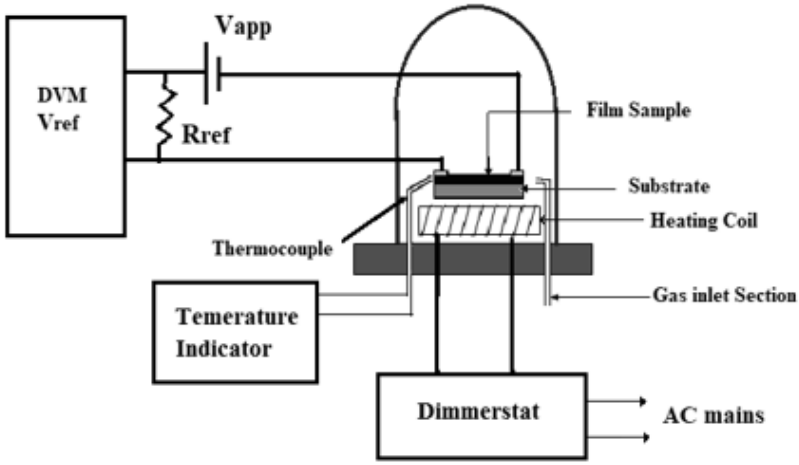

Fig. 6. Schematic diagram of static electric and gas sensing system.

The DC resistance of $LaCrO_3$ thick films was estimated using Eq. 3. The resistance versus temperature plots of unannealed and annealed $LaCrO_3$ thick films are shown in Fig. 7.

$$R\ sample = R\ ref\ [[(V\ supply) / (V\ ref)]-1] \quad (3)$$

Where, R sample is resistance of sample or film, R ref is reference resistor (10 M ohm), V ref is reference voltage across the sample.

Fig. 7 suggests that, as surrounding temperature of films is vary between the 280-640 K the resistance of films is changed. As surrounding temperature raised the resistance of both samples is deceased attributing negative temperature coefficient of resistance means semiconducting behavior of the films [20]. It is also observed that, the La2 sample shows more resistance at room temperature than La1 sample due to annealing process. The smaller crystallites alter electrical conductivity due to electron transport pathways along grain boundaries. The excessive grain boundaries can also act as scattering centers, reducing conductivity hence resistance is increased.

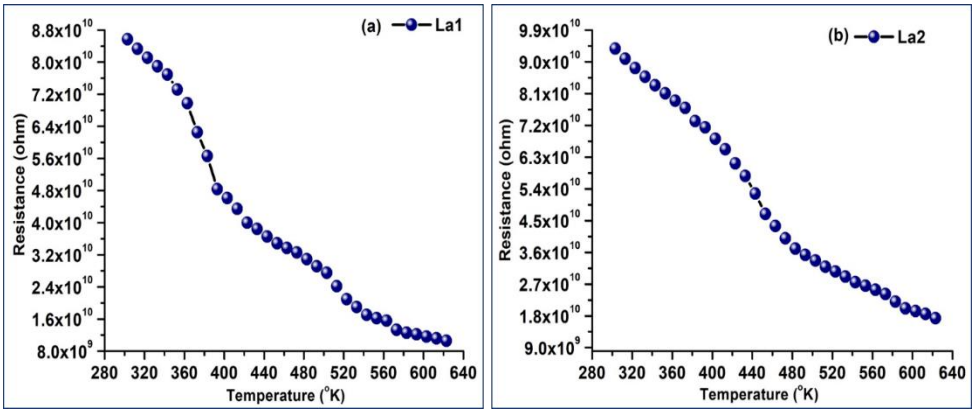

Fig. 7. Variation of resistance versus temperature plot of (a) unannealed and (b) annealed $LaCrO_3$ thick films.

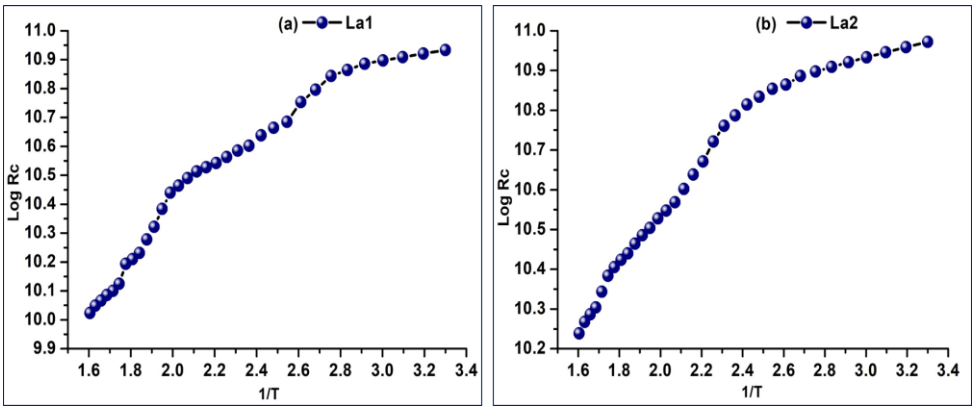

Fig. 8. Log R against 1/T for activation energy plot of (a) unannealed and (b) annealed $LaCrO_3$ thick films.

The resistivity and activation energy are the significant electrical properties and their magnitude plays vital role in the gas sensing mechanism. The resistivity, Temperature Coefficient of Resistance (TCR) and activation energy at higher temperature region (HTR) and lower temperature region (LTR) of $LaCrO_3$ thick films are calculated by using Eqs. 4-6 respectively [20,23]. The calculated electrical parameters magnitudes are tabulated in Table 3.

$$\text{Resistivity } (\rho) = (R \times b \times t)/l \quad (4)$$

Where, R is resistance at room temperature of sample, *l* is length of sample, b is width of sample, and t is thickness of sample.

$$TCR = 1/Ro\ (\Delta R/\Delta T)\ /^{o}C \quad (5)$$

Where, ΔR is change in resistance between temperature T_1 and T_2, ΔT is temperature difference between T_1 and T_2 and R_o is resistance of the film at room temperature.

$$\Delta E = \log R/\log Ro \times KT \quad (6)$$

Where, ΔE is activation energy, R is resistance at room temperature, R_0 is resistance at room temperature, K is Boltzmann constant and T is absolute temperature.

The activation energy in this region corresponds to the bandgap energy of the material. It is the energy required to move electrons from the valence band to the conduction band [22]. The estimated activation energy values for unannealed and annealed $LaCrO_3$ thick films are shown in Table 3. TCR is vary depending on the conduction mechanism. TCR is a crucial parameter for understanding how the electrical resistance of a material changes with temperature. It is especially important for materials used in sensors TCR is typically negative as resistivity decreases with temperature due to increased intrinsic carrier generation [21-23]. TCR is defined as the relative change in resistance per degree change in temperature. The TCR for unannealed and annealed $LaCrO_3$ thick films is -0.00372 and -0.00156/°C respectively. Table 3 shows the all estimated electrical outcomes of unannealed and annealed $LaCrO_3$ thick films.

Table 3. Electrical outcomes of unannealed and annealed $LaCrO_3$ thick films.

Sample	Thickness (μm)	Resistivity (Ω.m)	TCR (/°C)	Activation Energy (eV)	
				HTR	LTR
La 1	55	2356867	-0.00372	0.1751	0.0251
La 2	59	2765330	-0.00156	0.1061	0.0273

3.3. *Study of gas sensing properties of $LaCrO_3$ thick films*

Metal oxides are widely used in gas sensing applications due to their unique properties, such as high electrical conductivity, catalytic activity, and ability to interact with various gas molecules. The sensor's operating principle is based on the change in conductivity of the metal oxide when it interacts with gas molecules. The gas adsorption at the surface modifies the charge carrier density, leading to changes in resistance [23]. The gas sensing study was executed is display in Fig. 6. In the present research work the prepared $LaCrO_3$ thick films were tested to various gas like NO_2, CH_4, LPG, ethanol, NH_3 and petrol vapor. We continue to emphasize the need to monitor these gases using metal oxide sensors as all of these gas vapors are fatal and even small concentrations can be quite toxic. By using a thermostat to maintain a constant temperature inside the gas detection set up, gas residue was removed after each reading of gas sensing [24]. The sensitivity of $LaCrO_3$ thick films was calculated by utilizing Eq. 7. The sensitivity versus temperature plot of $LaCrO_3$ thick films is revealed in Fig. 9.

$$\text{Sensitivity} = Ra\text{-}Rg/Ra \times 100 \quad (7)$$

Where, Ra - Resistance of a thick film in air and Rg - Resistance of thick film presence of gas.

The prepared unannealed and annealed $LaCrO_3$ thick films show maximum sensitivity to NO_2 gas compared to other tested gases. The maximum sensitivity recorded for La1 and La2 samples is 68.19 % and 87.31 % respectively at 160 °C operating temperature. At 160 °C temperature, the thermal energy is sufficient to overcome activation barriers for adsorption and desorption processes, which is crucial for quick sensor responses. It is

observed that, the annealed thick films show the maximum sensitivity at lower ppm of NO_2 gas as compare to unannealed thick film samples.

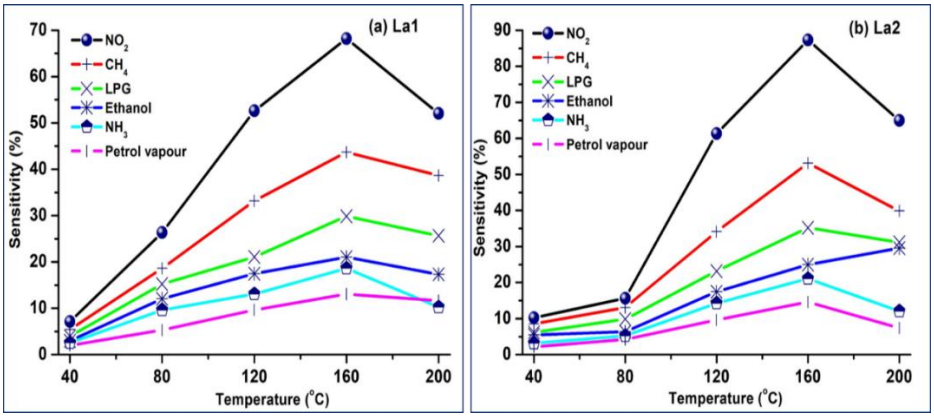

Fig. 9. Sensitivity versus temperature plot of (a) unannealed and (b) annealed $LaCrO_3$ thick films.

Annealing is a heat treatment process that can significantly affect the properties of thick films, such as $LaCrO_3$, enhancing their gas sensing performance [16]. Annealed thick films often show maximum sensitivity at lower concentrations of NO_2 gas compared to unannealed samples due to annealing temperature promote grain growth and modify the film's surface morphology, increasing surface roughness and porosity confirm by SEM analysis [20]. A higher surface area provides more active sites for gas adsorption. More adsorption sites mean that even at lower concentrations of NO_2, a significant number of gas molecules can interact with the film, increasing its sensitivity [20,23]. The selectivity of the $LaCrO_3$ thick films for a particular gas over others was estimated using Eq. 8.

$$\text{Selectivity} = S_{gas}/S_{target\ gas} \times 100 \quad (8)$$

Where, S_{gas} is sensitivity of interfering gas at an optimum operating temperature and $S_{target\ gas}$ is sensitivity of the target gas at the same temperature.

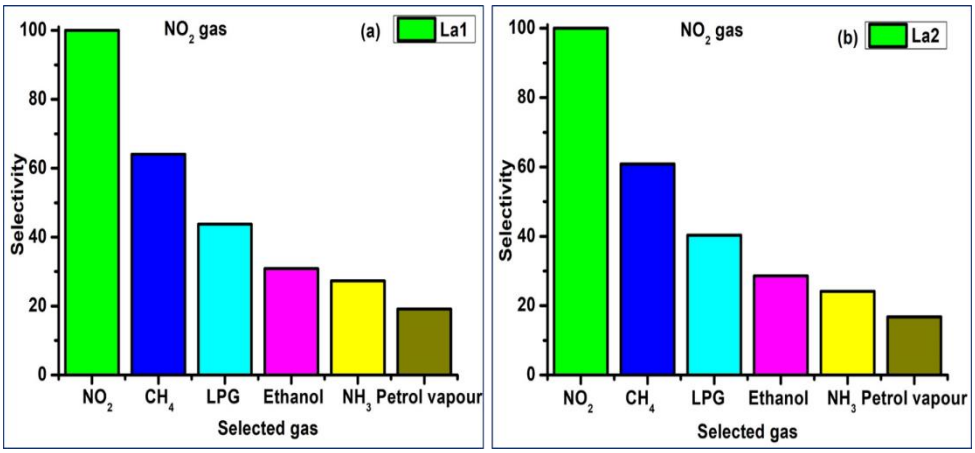

Fig. 10. Selectivity histogram for (a) unannealed and (b) annealed $LaCrO_3$ thick films.

Fig. 10 shows the selectivity histogram of $LaCrO_3$ thick films. The maximum selectivity was found to be to NO_2 gas. The defect states in $LaCrO_3$, such as oxygen vacancies, play a crucial role in enhancing the adsorption of NO_2 gas contributing to its selectivity [16,22].

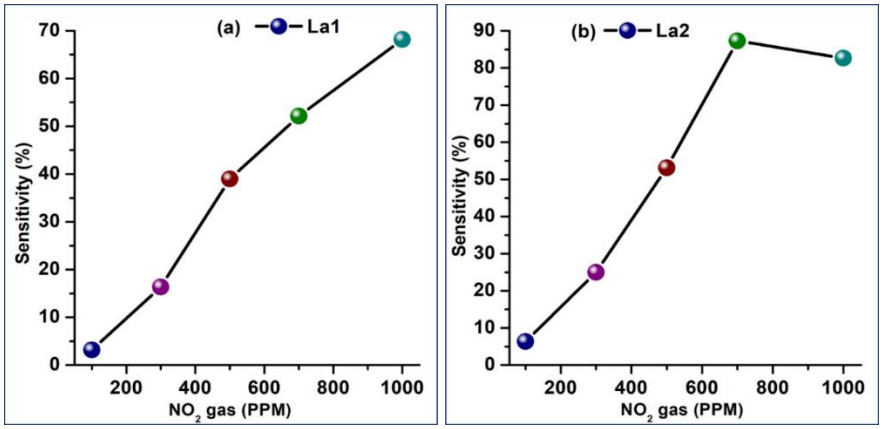

Fig. 11. Sensitivity versus NO_2 gas ppm plot of (a) unannealed and (b) annealed $LaCrO_3$ thick films.

Sensitivity versus NO_2 gas ppm plot of $LaCrO_3$ thick films is shown in Fig. 11. The La2 sample shows maximum sensitivity for 800 ppm concentration of NO_2 gas while La1 sample shows maximum sensitivity for 1000 ppm concentration of NO_2 gas. The La2 sample shows max sensitivity at lower temperature due to annealing process. The difference in maximum sensitivity to NO_2 gas between annealed and unannealed $LaCrO_3$ thick film samples can be attributed to the effects of the annealing process on the material's structure and properties. The improved properties of the annealed film, such as higher surface area, better crystallinity, and optimized defect states, contribute to higher sensitivity at lower temperatures [16,23]. This is because the enhanced interaction and adsorption of NO_2 molecules occur more effectively even at lower thermal energies. The unannealed sample requires a higher concentration of NO_2 (1000 ppm) to achieve maximum sensitivity due to lower surface area, higher defect density, and less optimized surface chemistry [25].

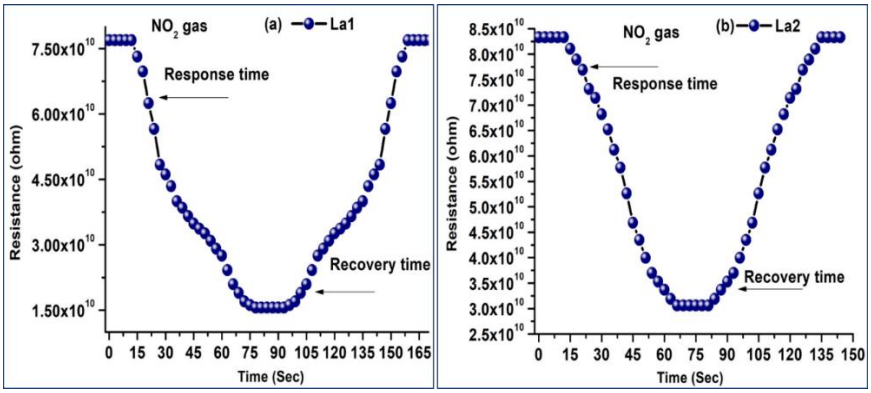

Fig. 12. Response and recovery curves for (a) unannealed and (b) annealed $LaCrO_3$ thick films.

Fig. 12 illustrate the response and recovery curves of $LaCrO_3$ thick films. The response and recovery time for unannealed sample was recorded 14 and 108 seconds respectively. While the response and recovery time for annealed sample was recorded 12 and 96 seconds respectively. The annealed sample shows the quick response and recovery time to NO_2 at operating temperature 160 °C as compared to unannealed $LaCrO_3$ thick films sample. Annealing increases the surface area and porosity of the films hence more porosity means gases can diffuse more quickly into and out of the film, improving both response and recovery times [25].

The reusability performance of $LaCrO_3$ thick films, whether annealed or unannealed, is an important aspect of their application in gas sensing. Reusability indicates the sensor's ability to consistently respond to repeated exposure to a target gas [16], such as NO_2, over multiple cycles. In this work, stability of sensor was tested by the run of 10 days up to 2 months. After each run the sensitivity of $LaCrO_3$ thick films was found to be decreased due to humidity and environmental or ambient conditions [25]. The sensitivity of La1 sample was decreased from 68.19 % to 64.41 % during the selected days. The sensitivity of La2 sample was also decreased from 87.31 % to 85.24 % during the selected days. La2 sample shows more stability the La1 sample. The annealing temperature has a profound effect on the stability of $LaCrO_3$ thick films. Optimal annealing temperatures enhance structural, electrical, and gas sensing stability by improving crystallinity, reducing defect density, optimizing surface area, and stabilizing electrical properties. Films annealed at these temperatures exhibit better mechanical integrity, consistent electrical behavior, stable gas sensing performance, and improved thermal resilience [25].

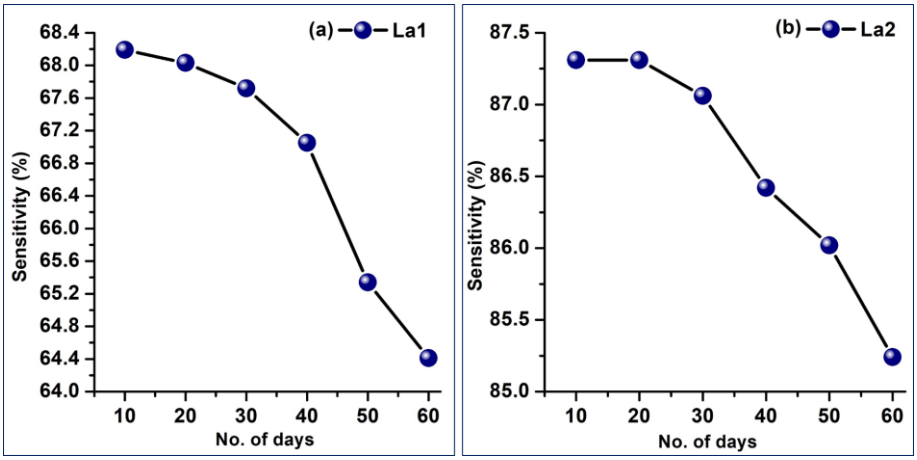

Fig. 13. Reusability performances of (a) unannealed and (b) annealed $LaCrO_3$ thick films.

The gas sensing mechanism of $LaCrO_3$ thick films to NO_2 gas is illustrate in Fig. 14. NO_2 is a strong oxidizing agent and has a high affinity for the oxygen vacancies and surface oxygen species present on $LaCrO_3$. This strong interaction leads to significant changes in the electrical properties of the film [26]. NO_2 molecules can chemisorb on the $LaCrO_3$

surface, which involves a transfer of electrons and a more stable interaction compared to physisorption, enhancing sensitivity [11]. The sensing mechanism is temperature-dependent. An optimal operating temperature, such as 160 °C, can enhance the adsorption-desorption kinetics and charge transfer processes, leading to improved sensitivity.

NO_2 is oxidizing gas and $LaCrO_3$ is p type semiconductor. When an oxidizing gas, such as NO_2, comes into contact with a p-type semiconductor, interactions occur at the surface. The oxidizing gas molecules adsorb onto the surface of the p-type semiconductor. This can occur via physisorption. In a p-type semiconductor, holes (positive charge carriers) are the majority carriers [20]. When the oxidizing gas captures electrons from the semiconductor, it effectively reduces the recombination of holes and electrons, leading to an increase in hole concentration [25,26]. The removal of electrons from the conduction band or from surface states leads to a relative increase in the number of holes (majority carriers) in the valence band. As the concentration of holes increases, the electrical conductivity of the p-type semiconductor increases, leading to a decrease in electrical resistance [28]. This is because the higher hole concentration improves the ability of the semiconductor to conduct electrical current. The change in resistance of $LaCrO_3$ thick films is consider as sensitivity of film [27-29].

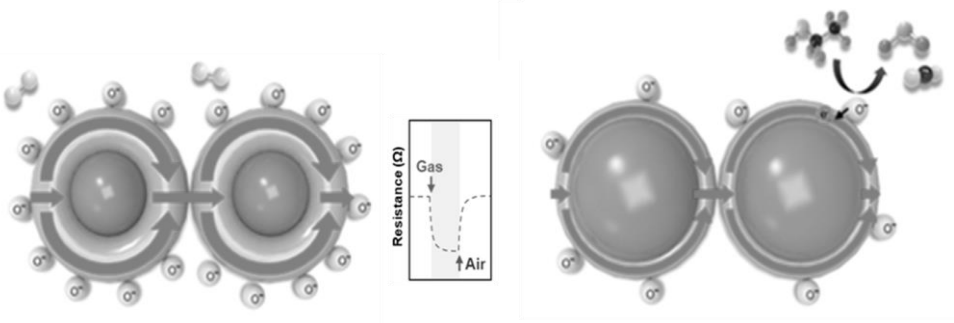

Fig. 14. Gas sensing mechanism of $LaCrO_3$ thick films to NO_2 gas.

4. Conclusion

$LaCrO_3$ nanoparticles were successfully synthesized using a less expensive sol-gel method. The $LaCrO_3$ thick films were developed on a glass substrate through a cost-effective screen-printing method. The impact of annealing temperature on $LaCrO_3$ thick films was studied, and it was found that annealing temperature strongly influences their electrical, structural, and gas sensing properties. The increase in peak intensity observed in the XRD pattern of $LaCrO_3$ with annealing temperature was attributed to improved crystallinity, reduction of defects, grain growth, increased phase purity, and annihilation of point defects. Due to the enhancement of adsorption sites, improved crystallinity, and better electrical properties, maximum sensitivity was achieved in the annealed sample at a lower NO_2 concentration of

800 ppm. It was observed that, the annealed $LaCrO_3$ thick films exhibited quicker response and recovery times to NO_2 at an operating temperature of 160°C compared to unannealed samples. This improvement was attributed to enhanced crystallinity, increased surface area, optimized surface chemistry, and improved electrical properties resulting from the annealing process. These modifications facilitated more efficient gas adsorption and desorption, leading to faster sensor performance. For applications requiring reliable and repeatable gas sensing performance, annealed $LaCrO_3$ thick films were found to be preferable. More consistent responses were demonstrated by annealed films over repeated cycles due to improved crystallinity and reduced defects, ensuring stable sensitivity and selectivity. The potential use of $LaCrO_3$ thick films for the detection and monitoring of NO_2 gas, as well as for the development of commercial gas sensors.

Acknowledgments

The authors thank to Principal, Research Centre in Electronic Science, Mahatma Gandhi Vidyamandir's Loknete Vyankatrao Hiray Arts, Science and Commerce College, Panchavati, Nashik-03, India, for providing laboratory facilities. The authors also acknowledge and pay sincere thanks to Head, Department of Physics and CIF S. P. Pune University, Pune for providing the laboratory facilities for SEM, EDX, and XRD characterization for present research work.

References

1. R. M. Al Jarrah, E. M. Kadhem, and A. H. O. Alkhayatt, Appl. Phys. A **128**, 527 (2022). https://doi.org/10.1007/s00339-022-05659-x
2. Y. Yang, B. Maeng, D. G. Jung, J. Lee, Y. Kim, J. Kwon et al., Nanomaterialas **12,** 3227 (2022). https://doi.org/10.3390/nano12183227
3. T. R. Acharya, D. K. Chaudhary, S. Gautam, A. K. Singh, R. Shrestha et al., Sens. Act. A: Phys. **351**, ID 114175 (2023). https://doi.org/10.1016/j.sna.2023.114175
4. S. H. S. Pai, A. Mondal, B. Ajitha, and Y. A. K. Reddy, Int. J. Hydrogen Energy **50**, 928 (2024). https://doi.org/10.1016/j.ijhydene.2023.07.345
5. F. Ghasemi, M. Ghasemi, L. Eftekhari, and V. Soleimanian, Optics Laser Technol. **146,** ID 107564 (2022). https://doi.org/10.1016/j.optlastec.2021.107564
6. P. Singh, F. M. Simanjuntak, L. L. Hu, T. Y. Tseng, H. W. Zan, and J. P. Chu, Sensors, **22**, ID 390 (2022). https://doi.org/10.3390/s22010390
7. N. A. Isaac, I. Pikaar, and G. Biskos, Microchim. Acta **189**, 196 (2022). https://doi.org/10.1007/s00604-022-05254-0
8. I. Koriba, B. Lagoun, A. Cheriet, A. Guibadj, S. Belhadj, A. Ameur, L. Aissani, and A. Alhussein, Appl. Phys. A **128**, 82 (2022). https://doi.org/10.1007/s00339-021-05150-z
9. J. A. Mena, V. Mendoza-Estrada, E. M. Sabolsky, K. A. Sierros, K. Sabolsky, R. González-Hernández, and K. S. V. Idhaiam, J. Eur. Ceramic Soc. **44,** 7040 (2024). https://doi.org/10.1016/j.jeurceramsoc.2024.04.062
10. W. Yin, W. Li, M. Li, Y. Cui, Y. Zhao, and Y. Chen, J. Sup. Novel Magnet. **35**, 1967 (2022). https://doi.org/10.1007/s10948-022-06293-7
11. V. S. Shinde, K. H. Kapadnis, A. P. Patil, and P. B. Koli, J. Ind. Chem. Soc. **99**, ID 100367 (2022). https://doi.org/10.1016/j.jics.2022.100367
12. M. Aamir, I. Bibi, M. Sabir, S. Mubarik, Q. Raza, A. M. Karam et al., Optical Mater. **145**, ID 114390 (2023). https://doi.org/10.1016/j.optmat.2023.114390

13. H. Zhao, Q. Zhu, X. Ye, L. Wang, and S. Dong, Coatings **14**, ID 147 (2024). https://doi.org/10.3390/coatings14010147
14. M. Javed, A. A. Khan, S. N. Khisro, A. Majeed, J. Kazmi, R. Bilkees et al., Mater. Chem. Phys. **290**, ID 126522 (2022). https://doi.org/10.1016/j.matchemphys.2022.126522
15. I. P. Morjan, E. Dutu, C. T. Fleaca, F. Dumitrache, I. Morjan, N. Mihailescu et al., Mater. Sci. Semicond. Proc. **142**, ID 106511(2022). https://doi.org/10.1016/j.mssp.2022.106511
16. P. S. Suryawanshi, A. V. Patil, G. G. Padhye, and U. J. Tupe, Adv. Mater. Res. **1180**, 67 (2024). https://doi.org/10.4028/p-uYHR0F
17. P. Prasad, S. Kiran, M. Meenu, and A. S. Prasad, Mater. Today: Proc. **80,** 1209 (2023). https://doi.org/10.1016/j.matpr.2022.12.200
18. A. A. Qahtan, N. Zarrin, M. Fatema, H. A. Al-Shamiri, W. Khan, and S. Husain, Physica Scripta **99**, ID 072001(2024). https://doi.org/10.1088/1402-4896/ad52f9
19. S. L. Wagh, U. J. Tupe, A. B. Patil, and A. V. Patil, Iranian J. Mater. Sci. Eng. **19** (2022).
20. S. S. Mandawade, R. V. Wagh, Yewale, C. R. Qadir, K. W. Abdullah, H. Y. Alharbi et al., J. Ind. Chem. Soc. **102**, ID 101514 (2025). https://doi.org/10.1016/j.jics.2024.101514
21. M. Akram, M. Rani, R. Shafique, K. Batool, M. A. Habila, and Sillanpää, M, J. Inorg. Organomet. Polym. Mater. **34**, 361 (2024). https://doi.org/10.1016/j.ceramint.2024.12.159
22. S. Wang, Z. Xu, F. Chen, S. Li, K. Bo, H. Guo et al., Ceramic Int. (2024). https://10.0.3.239/s10904-023-02814-6
23. S. C. Kulkarni, V. T. Salunke, S. Naeem, and A. V. Patil, Ceramic Int. (2025). https://doi.org/10.1016/j.ceramint.2025.01.077
24. A. Maria, I. Ahmad, S. Naeem, D. Husain, A. B. Patil, D. K. Halwar, and A. V. Patil, J. Ind. Chem. Soc. **101**, ID 101157 (2024). https://doi.org/10.1016/j.jics.2024.101157
25. M. H. Magar, V. A. Adole, M. R. Patil, R. H. Waghchaure, U. J. Tupe, and T. B. Pawar, J. Ind. Chem. Soc. **101**, ID 101396 (2024). https://doi.org/10.1016/j.jics.2024.101396
26. H. Sun, J. Song, P. Shi, Z. Cheng, L. Tian, M. Zhou, and T. Qi, J. Mater. Chem. A **12**, 18234 (2024). https://doi.org/10.1039/D4TA02809K
27. R. S. Ingale, S. G. Shinde, K. A. Khamkar, S. A. Ahire, and I. J. Patil, J. Phys.: Conf. Series **2426**, ID 012050 (2023). https://doi.org/10.1088/1742-6596/2426/1/012050
28. A. Mishra and R. Prasad, Catal. Rev. **56**, 57 (2014). https://doi.org/10.3329/jsr.v13i3.52435
29. G. Ravinder, J. Sci. Res. **13**, 347 (2021). https://doi.org/10.3329/jsr.v13i2.49333